PRAYAS

Students' Journal of Physics

volume 4 Number 4 Oct.-Dec. 2010

INDIAN ASSOCIATION OF PHYSICS TEACHERS

Editorial

Countering the Menace of Tutorial Homes

During the last couple of decades the traditional science education in general, and physics in purticular, has been undergoing steady erosion because of the evolution of a parallel system of education in the form of mushruming of tutorial homes in the country. Such institutions promise an easier path to gain entry into professional courses in all-India institutes like IITs and IISERs etc. through tailor-made training. The students leave the colleges and crowd in these institutions being lured of bright future.The science education imparted by the tutorial homes cannot be called education in the true sense of the terms, but anarrow specialised training to solve the problems normally set in the entrance tests. The theoretical foundation of the relevant formulae picked up from the text books for solving the problems and their historical evolution are hardly discussed or emphasised. Further, the laboratory practice to gain practical knowledge which form the core of science education does not form a part of the entrance tests, and therefore totally non-existent in the said training. Needless to say, such mercinary training of science is devoid of any potential to excite the imagination of the students and inspire them on creativity and innovativeness. The whole edifice of science education supported at its base by the plus-two level study suffers irrepairable damage.

Addressing recently the IITians in the Plan-IIT summit in New York, Narayan Murthy said that the quality of students entering IITs has deteriorated due to tutorial homes that prepare the engineering students. The majority of the students to the tune of 80 percent passing the IITs fare poorly at jobs and global instutes of higher education. Subsequently, directors of somr IITs have voiced similar sentiment. Such distorted education imparted by the tutorial homes imbues the mindset of the students with misplaced values and objectives about learning of science which continues to dominate their psyche in the UG and PG studies. A glairing fallout of this phenomenon is noticeable in the utter neglect of practicals and total lack of emphasis on labiratory practice reducing it to the level of ritual in university level. The cumulative effect has seriously affected the quality of physics education whose long term effect is fully incomprehensible presently.

How to counter the menace of tutorial homes ?

The Indian system of education originating in our colonial past is mostly based on rote learning and excellence in examination. It has stubernly defied any substantial innovation over the years. Teaching mainly consists in the delivery of the lectures by the teacher in the class room, and students taking down the notes for their preparation of the ensuing examinations. It is mostly a one-way traffic in which information/knowledge is expected to flow from the teachers to the students. It is

well recognised fact that knowledge flourishes the best when teaching is carried out in the medium of question-answer with full participation of teachers and students in an animated face-to-face discussion. In ancient India this was the principal mode of instruction as evidenced in the teaching of Bhagbat Gita, Srimad Bhagbat and Upanishad by Lord Krishna, Sukadev muni and Yagnabalkya to Arjuna, Parikhita and Maitryee respectively. In western countries regular tutorial classes form an integral part of science teaching, which is in general not the case in our country. Therefore, our science teaching is lack-lustre and fails to fire the imagination of the students and induce them to think creatively.

The present system of science education should be revamped with the introduction of tutorial class and mandatary number of seminars to be delivered by the student as a part of the curricula.The tutorial class could also cover the problems set in entrance tests, which are invariably an integral part of the course. In conjuction with this, regular conduct of practical classes with seriousness will surely be attractive to the students, and their dependence on the tutorial homes will gradually dwindle, finally coming to an end. This will equally benefit the teachers by enhancing their knowledge and insight in the subject which may culminate in some research work. It is often said that the best way to learn is to teach. The classic case of the legendary teacher and great physicist Richard Feynmann may be worth recalling here, who preferred to work at Cornell university rather than join a more prestigious post in Institute of Advanced Studies Princton lured by the prospect of teaching in undergraduate classes in the former.

L. Satpathy

P R A Y A S
Students' Journal
of Physics

TURNING POINTS

The Big Bang and the Little Bang

Rajeev S. Bhalerao*
Department of Theoretical Physics, Tata Institute of Fundamental Research, Mumbai 400 005, India

Communicated by: D.P. Roy

1. INTRODUCTION

What is the world made of? Or, what are the ultimate constituents of matter? Mankind has asked these questions since ages. Answers have varied from time to time. What were thought to be the ultimate constituents of matter at one time, turned out to be not so with the passage of time and the advancement of knowledge. A related question is how do the ultimate constituents of matter interact with each other, or in other words, what are the basic or fundamental interactions in physics. Another equally profound question is how and when did the universe come into existence. Again the answers have changed with the progress of science. Interestingly, it turns out that these questions and these issues are interlinked: The science of the "big", that is, the study of the origin and evolution of the universe – cosmology – is deeply intertwined with the science of the "small" – the elementary particle physics. Tremendous progress has been made in the last few decades towards seeking answers to these questions. Of course, the quest is far from over. This article is an attempt to introduce the undergraduate student of science to these exciting developments.

The "Big Bang" in the title, of course, refers to the most-accepted theory of the origin of the universe, and the "Little Bang" refers to the collision of two atomic nuclei in the laboratory, at ultra-relativistic energies: By ultra-relativistic energies one means energies so high that each of the two colliding nuclei has an energy far greater than (say, 10 or 100 times) its rest mass. According to Einstein's Special Theory of Relativity, such energies are attained when particles move with speeds

*bhalerao@tifr.res.in

approaching the speed of light [1]. When two nuclei collide with each other at such high energies, they are completely destroyed. The collision gives rise to a high energy density fireball with a temperature of the order of 10^{12} K [2], albeit over a small region and for a short interval of time. At such high temperatures matter exists in a state called quark-gluon plasma (to be defined later). The early universe, about a microsecond after the Big Bang, existed in such a state. Thus the collision of two nuclei at ultra-relativistic energies recreates conditions similar to those which existed soon after the Big Bang, hence the name the "Little Bang".

Let us go back to the three questions raised in the first paragraph. Our present understanding of the ultimate building blocks of matter is summarized in Fig. 1. Quarks come in six varieties: up (u),

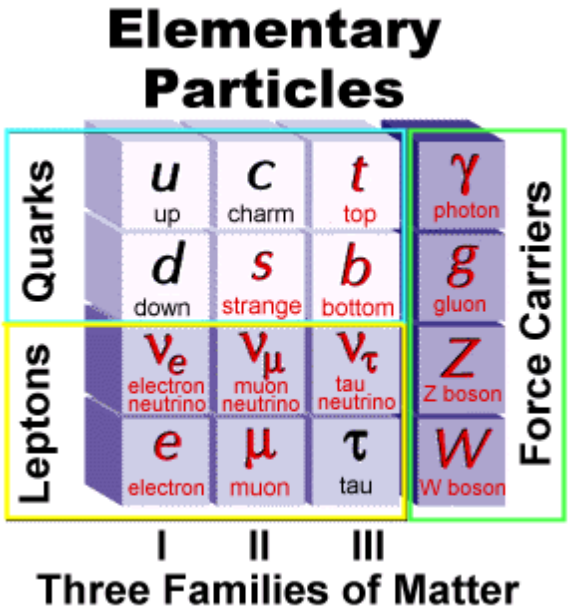

Figure 1. Ultimate building blocks of matter.

down (d), strange (s), charm (c), bottom (b) and top (t). These are just the names given to the quarks and nothing much should be read into them. These are also called the six flavours of the quark. In addition, there are six types of leptons, namely electron (e), muon (μ), tau (τ), electron neutrino (ν_e), muon neutrino (ν_μ), and tau neutrino (ν_τ). The six types of leptons together with the six types of quarks are arranged in three columns: u, d, ν_e, e in the first column, c, s, ν_μ, μ in the second column, and t, b, ν_τ, τ in the third column. These are called the three families or three generations of matter. There are also antiparticles corresponding to these 12 particles, e.g., $\bar{u}$ is the antiparticle of

[1] Show that for the total energy to be 10 or 100 times the rest mass, the speed has to be about 0.995 or 0.99995 times the speed of light, respectively.

[2] In comparison, the temperature at the centre of the sun is about 1.6×10^7 °C.

u. Most of the matter that we see around us is essentially made of u, d, and e: uud makes a proton, ddu makes a neutron, protons and neutrons together make the atomic nucleus which together with electrons makes an atom, and atoms make molecules. Molecules, atoms, electrons, nuclei, protons and neutrons can exist in isolation or as free particles. However, quarks and antiquarks (and gluons which are introduced in the next paragraph) cannot exist in isolation under normal circumstances. This is the hypothesis of confinement. Confinement is not fully understood theoretically, but there is no experimental evidence to contradict the hypothesis.

Our second question was about the basic interactions. These are gravitational, electromagnetic, strong nuclear and weak nuclear. Elementary particles interact among themselves by exchanging particles called the *force carriers*. These are shown on the right-hand side of Fig. 1: photon (γ) for the electromagnetic, gluon (g) for the strong nuclear, and Z and W for the weak nuclear interactions. Force carrier for the gravitational interaction (graviton) is not yet discovered. Unification of electric and magnetic interactions into one electromagnetic interaction was achieved in the 19th century. Quantum electrodynamics (QED) is the modern theory of the electromagnetic interactions. It is a highly successful theory. Unification of electromagnetic and weak nuclear interactions was achieved in the 1960's. That theory is called the electroweak theory. Quantum Chromodynamics (QCD) is the theory of the strong nuclear interactions. It is thought that there is actually only one basic interaction and the above four are merely its manifestations at low energies. It is expected that at extremely high energies, these four interactions will be unified into one fundamental interaction. Attempts are underway to construct such a theory.

All evidence [3] indicates that the Big Bang occurred and the universe came into existence about 13.7 Billion years ago [4]. Since then, the universe has been expanding and cooling. Figure 2 shows the (average) temperature of the universe versus the time elapsed after the Big Bang. At time $\sim 10^{-6}$ sec, the universe was too hot for bound states of quarks to exist. As it cooled, quarks, antiquarks and gluons could combine to form hadrons (i.e., the strongly interacting particles such as protons, neutrons, etc.). As the temperature decreased further, protons and neutrons (collectively called the nucleons) combined to form nuclei. Atoms came into existence much later. The temperature today is about 2.7 K. Relativistic Heavy-Ion Collider (RHIC) is the name of the experimental facility at the Brookhaven National Laboratory, New York, USA which accelerates nuclei to ultra-relativistic energies, lets them collide with each other and observes the end-products with the help of special particle detectors. As stated above, such collisions are expected to produce matter at temperatures

---

[3] Evidence for the Big Bang theory: (a) Hubble-type expansion seen in red-shifts of the galaxies, (b) observed microwave background radiation, especially its detailed shape, (c) observed abundances of the light elements such as ${}^2H,\ {}^{3,4}He,\ {}^7Li$.

[4] To appreciate how big this number is, imagine that the Big Bang occurred exactly one year ago. On this time-scale, the solar system came into existence about 4 months ago, life originated on the earth about 3 months ago, dinosaurs appeared a week ago and vanished 2 days ago, anatomically modern humans appeared on the scene 6 minutes ago, the pyramids were built 10 seconds ago, and Christofer Columbus set out to "discover" India only 1 second ago!

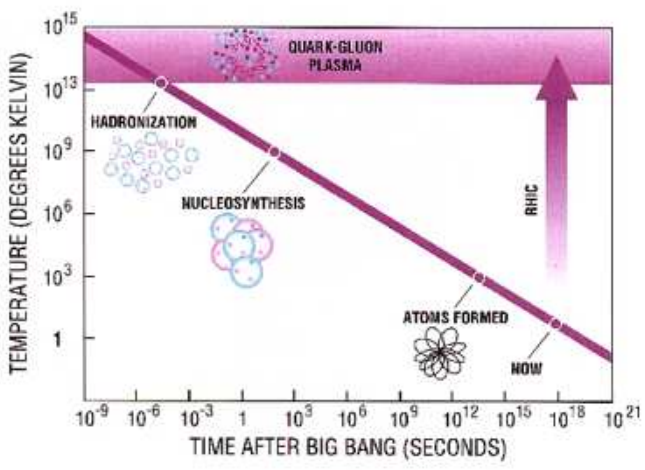

Figure 2. Temperature history of the universe.

of the order of 10^{12} K. QCD predicts that at such high temperatures, matter exists in a state called quark-gluon plasma (QGP). This is defined as a (locally) thermally equilibrated state of matter in which quarks, antiquarks and gluons are not confined to individual protons or neutrons but instead propagate over a region which is much larger: nucleon radius is ~ 1 fm, whereas the radius of QGP formed in a nucleus-nucleus collision may be ~ 10 fm (1 fm = 10^{-13} cm).

2. QCD PHASE DIAGRAM

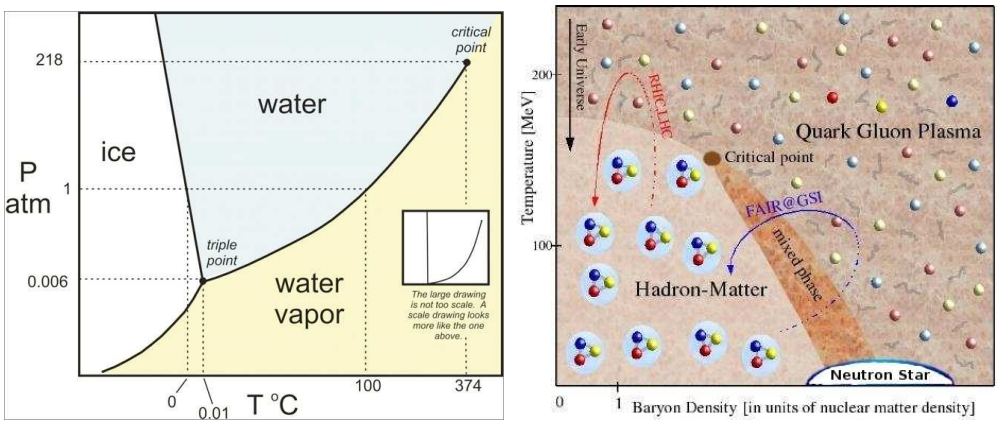

Figure 3. (a) Phase diagram of water, and (b) QCD phase diagram

Figure 3 presents the phase diagram of water on the left and the QCD phase diagram (i.e., the phase diagram of strongly-interacting matter) on the right. The former is very well-studied and its

various features are known quite accurately. The QCD phase diagram in contrast is not so well understood. The vertical axis in Fig. 3(b) shows the temperature T in MeV; one MeV is about 10^{10} K. We have seen that hadrons are the strongly interacting particles. Hadrons (such as protons, neutrons, etc.) made of three quarks are called baryons, and hadrons (such as pions, kaons, etc.) made of a quark and an antiquark are called mesons [5]. A large nucleus (such as gold, lead, or uranium) has a density of about 2×10^{17} kg/m^3 at its centre. The horizontal axis in Fig. 3(b) gives the net baryon density in these units, so the '1' marked on the horizontal axis is where an ordinary nucleus would be. The net baryon density means the density of baryons minus the density of antibaryons. At low temperatures and densities the matter exists in the hadronic state, i.e., the degrees of freedom are hadrons. At high temperatures and/or densities one expects the existence of QGP where the degrees of freedom are quarks, antiquarks and gluons. (These are collectively called the *partons*.) Neutron stars have densities much higher than the ordinary nuclei, and it is speculated that the deconfined matter may exist in the core of the neutron star. Figure 3(b) indicates the hadronization transition [6] that the early universe underwent at $T \sim 175$ MeV and a very small net baryon density. RHIC, LHC, FAIR are the names of the experimental facilities which probe (or will probe) other regions of the phase diagram. Critical point is the point at which the phase boundary ceases to exist (see also Fig. (3a)). Above the critical point there is no sharp distinction between the two phases, only a smooth crossover. Coordinates of the critical point in Fig. 3(a) are well-determined. In contrast, the existence of the critical point in Fig. 3(b), although expected theoretically, is not yet demonstrated experimentally.

This is the "Big Picture": The aim is to map out quantitatively the QCD phase diagram, and the relativistic heavy-ion collisions serve as an experimental tool for this purpose. It is a messy tool no doubt, but it is the only tool available to us.

3. RELATIVISTIC HEAVY-ION COLLIDER - RHIC

RHIC, BNL started operating in the year 2000 and since then has produced a wealth of data on gold-gold ($AuAu$), deuteron-gold (dAu) and proton-proton (pp) collisions at various energies. One does not expect the formation of QGP in dAu and pp collisions because the resulting systems are too small to allow multiple collisions among the deconfined partons. (Note that the multiple collisions are necessary for a many-body system to attain local thermal equilibrium.) These latter data only serve as baseline measurements which are used to decide whether there is any new physics in $AuAu$ collisions. The maximum energy to which each Au nucleus can be accelerated at RHIC is $100A$ GeV, where $A = 197$ is the mass number of the Au nucleus. At this energy, each $AuAu$ collision produces many hundreds of particles. Figure 4 shows the tracks left behind by these particles in

[5] Actually these are only the *valence* quarks or antiquarks. Hadrons, in addition, contain gluons and a number of quark-antiquark pairs, collectively called the *sea* quarks.

[6] This is not strictly a phase transition, but a smooth crossover.

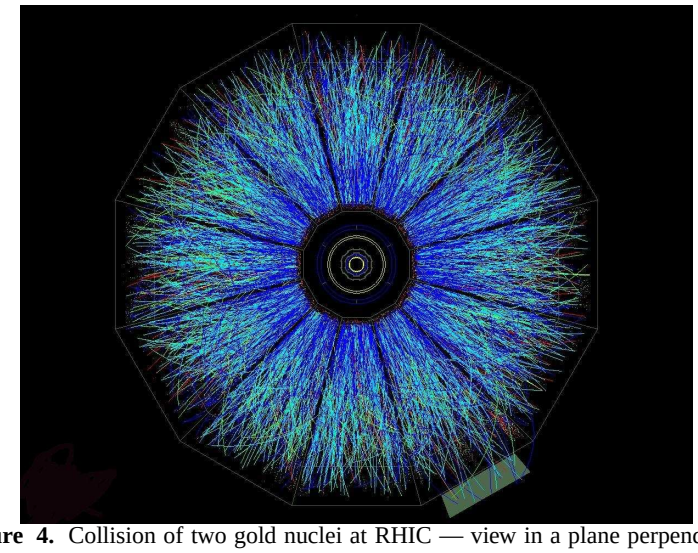

Figure 4. Collision of two gold nuclei at RHIC — view in a plane perpendicular to the beam axis.

one such collision event. Among the particles that are produced as an aftermath of the collision are photons, pions, other mesons, protons, neutrons, etc. Particle detectors at RHIC identify these particles and measure their energies and momenta event by event. Quark-gluon plasma if formed has a spread of about 10 fm from the point of collision and a lifetime of about 10^{-23} sec, after which quarks and gluons recombine to give rise to the particles listed above. And it is these particles which reach the detectors, not quarks and gluons. Analysing these data to deduce whether QGP was formed in an event, is clearly a non-trivial task, far more difficult than detecting the proverbial needle in a haystack.

The RHIC data when analysed, show clearly that the highest temperature attained at RHIC is sufficient to cause a transition to the region marked Quark-Gluon Plasma in Fig. 3(b). The temperature is determined by detecting photons emitted by the fireball very early in the collision event [7]. Among the most interesting findings at RHIC was the observation that the QGP behaves like an almost perfect fluid. In fact, no other fluid ever studied in the laboratory is as perfect as this fluid. This means that it has the smallest ever observed coefficient of shear viscosity (measured in units of the entropy density) [8]. Another important observation at RHIC goes by the name of *jet quenching*:

---

[7] This is similar to estimating the temperature of a hot iron rod by knowing whether it is red or yellow or white.

[8] In nonrelativistic fluid dynamics, the kinematic viscosity (ν) is defined as $\nu = \eta/\rho$ where η is the coefficient of shear viscosity or the dynamic viscosity and ρ is the density of the fluid. It allows us to compare the viscosities of fluids with different densities. (Interestingly, under standard conditions, water has a *lower* ν than air, although its η is higher.) The dimensionless ratio η/s, where s is the entropy density, serves as the relativistic analog of the kinematic viscosity.

a high-energy parton loses energy as it passes through QGP. Study of jet quenching throws light on the properties of the hot and dense medium through which the parton propagates.

What remains now is to carefully study and quantify the properties of this fluid. In order to locate the critical point and the phase transition line separating the hadron matter phase and the QGP phase (Fig. 3(b)), RHIC has been colliding gold nuclei over a range of energies. Plans are afoot to perform similar studies at FAIR (GSI, Germany) and NICA (JINR, Russia).

4. LARGE HADRON COLLIDER - LHC

The Large Hadron Collider at the European Organization for Nuclear Research (CERN), Geneva, Switzerland has started operating in November 2009. Presently it is operating in the proton-proton mode, but plans to collide lead (Pb) nuclei on each other, sometime in 2011. Here are some fascinating facts about the LHC:

It is the world's largest and most powerful particle accelerator. The accelerator is in a circular tunnel which is about 27 km in circumference and about 100 m underground. It accelerates protons and nuclei; the maximum design energy for the proton beam is 7 TeV and for the lead beam 2.7A TeV. Here $A = 208$ is the mass number of the lead nucleus. It uses 9300 superconducting magnets to guide the beams along the tunnel and focus them. It needs 10080 tonnes of liquid nitrogen and 60 tonnes of liquid helium to cool the magnets. Thus it is the largest refrigerator in the world. The beams move in an ultra-high vacuum, the pressure being maintained is 10^{-13} atm. At the full design power, trillions of protons go around the tunnel about 11245 times a second [9]. About 600 million proton-proton collisions occur per second. Each head-on collision creates a fireball with temperature of the order of 10^{12} K, to be contrasted with the extreme cold, -271.3 $^{\circ}$C (1.9 K), under which the superconducting magnets operate. Thousands of particles are produced in every collision. To detect these particles (typical size 10^{-13} cm or smaller and mass 10^{-27} kg or smaller), identify them, and measure their energy-momenta, LHC employs huge particle detectors. The heaviest among them, called a Compact Muon Solenoid (CMS), is 21 m long, 15 m across and weighs 12500 tonnes. It generates a magnetic field of 4 teslas, about 100000 times that of the earth. LHC will produce 15 petabytes (15 million gigabytes) of data annually, equivalent to 1.7 million dual-layer DVDs a year. To store and analyze this mass of data, LHC will use the *Worldwide LHC Computing Grid* which is a network of computers spread over 34 countries. TIFR (Mumbai) and SINP/VECC (Kolkata) have computers which are part of this network. Many scientists from several institutions in India have been participating in the experiments at RHIC as well as LHC.

---

[9] Show that a 7 TeV proton will indeed go around the LHC tunnel about 11245 times a second.

4.1. Why LHC?

LHC is expected to throw light on many fundamental questions such as:

• What is the origin of mass? Does the theoretically predicted Higgs boson (which endows particles with mass) really exist? If found, it would be an additional building block in Fig. 1.

• What is 96% of the universe made of? (The stars, galaxies, and everything else that we observe in the universe make only about 4% of its mass.)

• Supersymmetry provides an attractive extension of the standard model of particle physics. It predicts that for every particle in Fig. 1, there is a supersymmetric partner. But these have never been observed possibly because of their heavy mass. Is the LHC energy enough to produce some of these particles and thus provide support to the idea of supersymmetry?

• The Big Bang must have created equal amounts of matter and antimatter. Why is there more matter than antimatter in the present-day universe?

• Are there more than three space dimensions as required by the string theory?

• What was the universe like when it was just about 1 microsecond old?

4.2. Speculative "Doomsday Scenarios"

The LHC, right from its commissioning stage, faced opposition from some quarters. The Big Bang created the universe, the Little Bang may destroy it — so claimed the opponents. They anticipated and feared the following doomsday scenarios:

• Formation of a stable microscopic black hole that accretes ordinary matter.

• Formation of a stable *strangelet*, a hypothetical chunk of matter containing roughly equal numbers of u, d, s quarks, that accretes ordinary matter.

The CERN appointed a team of eminent independent scientists to examine these candidate mechanisms which were supposed to result in the destruction of the earth and the mankind. The team examined these possibilities carefully, and firmly excluded them on empirical or theoretical grounds or both:

Microscopic black holes, if produced, are expected to evaporate quickly by emitting energy by the quantum mechanical process called the Hawking radiation. Even if they are stable, they would not be dangerous to the earth for the following reason. Cosmic rays have been bombarding the earth and denser astronomical bodies such as the neutron stars and white dwarfs for billions of years. Some of the cosmic rays have energies far greater than the LHC energy. In other words, collision events such as those planned at LHC, have been occurring naturally in the universe, for billions of years, without any catastrophic consequences to the earth and the other heavenly bodies.

As for the formation of stable strangelets, the probability of their production decreases with energy. Because they have never been seen in the previous lower-energy experiments, they are unlikely to be produced at LHC. Moreover, they cannot be stable at high temperatures such as those expected at LHC.

Thus the LHC experiments present no danger and there are no reasons for concern.

5. THE BIG BANG AND THE LITTLE BANG - COMPARISION

The Big Bang happened and the universe was born about 13.7 billion years ago. That is one experiment we cannot repeat in the laboratory. But we can collide two large nuclei on each other at ultrarelativistic energies and study the resulting Little Bang.

(a) In either case, we do not know for sure what the initial state was; we only have plausible scenarios. They describe how the initially non-thermal system converts itself into one with local thermalization. This happened $\sim 10^{-35}$ sec after the Big Bang and happens $\sim 10^{-24}$ sec after the Little Bang. Thus the thermal era sets in.

(b) In each case, the system continues to expand and cool. The expansion is governed by the appropriate equations of motion and the appropriate thermodynamic equation of state.

(c) As the universe cools, it undergoes the electro-weak phase transition: electroweak unification breaks down, and electromagnetic and weak interactions acquire their separate identities [10]. Further on, it undergoes the QCD transition or the hadronization (see Fig. (3b)). In the case of the Little Bang, only the QCD transition takes place.

(d) Eventually, in the former case, first the neutrinos and then the photons decouple from the matter, i.e., they start propagating with almost no interaction with the matter. This gives rise to the cosmic neutrino background (CνB) and cosmic microwave background (CMB). In the case of the Little Bang, as the fireball cools enough, hadrons decouple from each other; the process is also known as the freezeout.

(e) Although the initial conditions are uncertain, we can observe the final state, work our way backwards in time, and thus try to learn about the initial state. Theoretical models of the initial state and the subsequent evolution of the system contain several free parameters which are fitted to reproduce the observed final state. That is the general program followed in the case of the Big Bang as well as the Little Bang.

The unknown parameters in the former case are the age of the universe, the age of decoupling, the Hubble constant (the ratio of the recession velocity of a distant star or galaxy with its distance from the earth), baryon to photon ratio, baryon density, dark matter density, etc. Analogously, in the latter case, the unknown quantities are the initial energy density distribution, thermalization time, initial temperature, decoupling or freezeout temperature, etc. The main final-state observables in the case of the Big Bang are the CMB radiation and its anisotropy. In the case of the Little Bang also the anisotropy of the distribution of hadrons, in the plane transverse to the beam axis, plays a crucial role.

(f) It is thought that the early universe developed "bubbles" inside which certain symmetries were broken, and as a result, there is more matter than antimatter in the present-day universe. There are

---

[10] After the Big Bang, the gravitational interaction separated first from the strong and electroweak interactions. Later on, the strong interaction separated from the electroweak interaction. But these processes occurred even earlier than 10^{-35} sec.

hints of a similar effect at RHIC: QGP formed in certain collisions is seen to have “bubbles” in it. These are the regions in which the mirror symmetry (called parity) may be violated.

Cosmology and ultra-relativistic heavy-ion physics are both very challenging and active areas of research today. Data on CMB radiation from the satellites namely COBE, WMAP and Planck, launched in years 1989, 2001, 2009 respectively, have been contributing enormously to the progress in cosmology. These data allow us to test our theories of the early universe and the origin of cosmic structure. In parallel with this, data from the heavy-ion accelerator facilities namely SPS (Super Proton Synchrotron at CERN), RHIC and LHC, commissioned in 1987, 2000, 2009 respectively, have been giving insights into the formation and evolution of the quark-gluon plasma, an important feature of the QCD phase diagram.

P R A Y A S
Students' Journal
of Physics

Dimerized Ising chain: two point correlation

Aritra De
Second Year, Physics Department, NISER, Bhubaneswar, India

Abstract. The free energy of an elastic Ising chain, with a dimerizing distortion, in an external magnetic field has been calculated earlier. The free energy exhibits a tricritical point. In this paper, we calculate the spin-spin correlation in this model.

Communicated by: L. Satpathy

1. INTRODUCTION

One of the most influential model of a system capable of a phase transition is the Ising model. This was invented by Wilhelm Lentz. He gave his student, Ernst Ising, this model as a problem to solve. For the one dimensioal case, Ising solved it in 1925. The solution of this model in two dimensions is due to Lars Onsager. By solving it exactly, in the absence of external magnetic field, he studied the behaviour of various correlations near the phase transition point. This was in 1944. Unlike the first order Ising model, for the two dimensional one, phase transition occurs at finite temperature. Despite years of intensive effort, an exact solution of the Ising model in three dimensions or in two dimensions with external magnetic field is still lacking. Our focus, in this paper, will be a distorted version of one dimensional Ising model. But before going to it, let us introduce the original Ising model in one dimension.

Consider a one dimensional lattice or chain. We will consider a very long chain and identify the two ends of this chain. At each lattice sites spin variables S_is are sitting which can be up or down. The other way of parametrizing this is to assign $+1$ for spins pointing up and -1 for those pointing down. The subscript i is the index identifying the lattice site at which S_i is sitting. The Hamiltonian of the system is given by

$$H = -J \sum_i J S_i S_{i+1} - h \sum_i S_i, \tag{1}$$

with $J > 0$. Clearly there are only interactions between neighbouring spins and the strength of the interaction is controlled by the coupling J. In the above equation, h represents an external magnetic field. Computing the partition function and the free energy exactly, it can be shown that the sistem shows a critical behaviour near $T = 0$. There are excellent discussions of this model in many

introductory text books on statistical mechanics. We refer to the reader the book by Baxter [1]–the calculational techniques of which we will follow throughout.

Though the Ising model in one dimension does not show a phase transition at finite temperature, it is possible to distort the model inducing interesting phase structures. Transitions between them are then controlled by temperature and other parameters of the model. One such model, which will be the focus of this article, is the dimerized Ising chain. Interestingly, this model has a tricritical point in its phase diagram [2]. A simple description of this model was provided in [3]. Our aim in this note is to provide a calculation of the two point correlator of this model. Further, analyzing the behaviour of the correlator, we identify the critical point where correlation length diverges.

We begin by introducing the model following [3].

1.1. The model

The Hamiltonian is given by:

$$H = -J_0 \sum_i (S_i S_{i+1}) - J_1 \epsilon \sum_i ((-1)^i S_i S_{i+1}) - h \sum_i S_i + N\omega_0 \epsilon^2. \tag{2}$$

Here

- N is the number of spin variables. These variables take values $S_i = \pm 1$. The sum is over the chain sites.
- J_0 is the exchange constant.
- J_1 is the first derivative of J_0 with respect to the distance between the spins.
- ω_0 is the frequency of dimerized distortion.
- ϵ is the lattice distortion resulting in long and short bond lengths between adjacent spins. The term $N\omega_0\epsilon^2$ has been introduced to stabilize the model.

The lattice distortion parameter ϵ causes alternating long and short bonds between neighbouring spins. This results in alternating nearest-neighour coupling constants $J_0 \pm \epsilon J_1$. This distortion is known as the dimerizing lattice distortion. By introducing two matrices,

$$F = \begin{pmatrix} e^{\beta(J_0+\epsilon J_1)+\beta h} & e^{-\beta(J_0+\epsilon J_1)} \\ e^{-\beta(J_0+\epsilon J_1)} & e^{\beta(J_0+\epsilon J_1)-\beta h} \end{pmatrix} \tag{3}$$

and

$$G = \begin{pmatrix} e^{\beta(J_0-\epsilon J_1)+\beta h} & e^{-\beta(J_0-\epsilon J_1)} \\ e^{-\beta(J_0-\epsilon J_1)} & e^{\beta(J_0-\epsilon J_1)-\beta h} \end{pmatrix} \tag{4}$$

the partition function

$$Z = \sum_{S_i} e^{-\beta H} \tag{5}$$

can be brought to a form

$$Z = \mathrm{Tr}[(FG)^{N/2}]. \tag{6}$$

Since this has been already discussed in [3], we have been very brief here. The explicit form of FG follows from (3) and (4) and we record it here for later use.

$$FG = \begin{pmatrix} \frac{1}{A} + AB^2 & B\sqrt{C} + \frac{1}{B\sqrt{C}} \\ \frac{B}{\sqrt{C}} + \frac{\sqrt{C}}{B} & \frac{1}{A} + \frac{A}{B^2} \end{pmatrix}. \tag{7}$$

Here we have defined

$$A = e^{2\beta J_0}, \;\; B = e^{\beta h}, \;\; C = e^{4\epsilon\beta J_1}. \tag{8}$$

The eigenvalues of the matrix (7) are

$$\begin{aligned} \lambda_1 &= \Big(\frac{1}{A} + \frac{A}{2B^2} + \frac{AB^2}{2} - \sqrt{\frac{A^2C + 4B^2C + 4B^6C + A^2B^8C + B^4(4 - 2A^2C + 4C^2)}{4B^4C}}\Big) \\ \lambda_2 &= \Big(\frac{1}{A} + \frac{A}{2B^2} + \frac{AB^2}{2} + \sqrt{\frac{A^2C + 4B^2C + 4B^6C + A^2B^8C + B^4(4 - 2A^2C + 4C^2)}{4B^4C}}\Big). \end{aligned} \tag{9}$$

Note that $\lambda_1 < \lambda_2$. The matrix which diagonalizes FG is given by

$$D = \begin{pmatrix} D_1 & D_2 \\ 1 & 1 \end{pmatrix}, \tag{10}$$

where

$$\begin{aligned} D_1 &= -\frac{A\sqrt{C} - AB^4\sqrt{C} + \sqrt{4B^4 + A^2C + 4B^2C - 2A^2B^4C + 4B^6C + A^2B^8C + 4B^4C^2}}{2B(B^2 + C)}, \\ D_2 &= -\frac{A\sqrt{C} - AB^4\sqrt{C} - \sqrt{4B^4 + A^2C + 4B^2C - 2A^2B^4C + 4B^6C + A^2B^8C + 4B^4C^2}}{2B(B^2 + C)}. \end{aligned} \tag{11}$$

The partition function then becomes

$$Z = \lambda_1^{\frac{N}{2}} + \lambda_2^{\frac{N}{2}} \tag{12}$$

Then the free energy per site in the thermodynamic limit is given by

$$F = -\frac{1}{\beta} \lim_{N\to\infty} \ln Z = -\frac{1}{2\beta} \ln \lambda_2. \tag{13}$$

up to some additive ϵ^2 term [3].

In the next section, we present our computation of two point spin-spin correlation in this model. This follows the technique of [1].

2. CALCULATION OF THE TWO-POINT CORRELATION FUNCTION

Let us consider the two point correlation $< S_1 S_3 >$ for example. This is given by

$$< S_1 S_3 >= Z^{-1}\mathrm{Tr}[\mathcal{S}(FG)\mathcal{S}(FG)^{\frac{N}{2}-1}] \tag{14}$$

where we have introduced $\mathcal{S}$ as a two by two matrix

$$\mathcal{S} = \begin{pmatrix} 1 & 0 \\ 0 & -1 \end{pmatrix} \tag{15}$$

Therefore, in general, we have (for $j-i$ even, $j > i$, the case where $j-i$ odd will be considered later.)

$$< S_i S_j >= Z^{-1}\mathrm{Tr}[\mathcal{S}(FG)^{\frac{j-i}{2}}\mathcal{S}(FG)^{\frac{N}{2}-\frac{j-i}{2}}] \tag{16}$$

Denoting $j-i=\alpha$ with α even, we finally have

$$< S_i S_j >= Z^{-1}\mathrm{Tr}[\mathcal{S}(FG)^{\frac{\alpha}{2}}\mathcal{S}(FG)^{\frac{N-\alpha}{2}}]. \tag{17}$$

Also it easily follows that the one point function is given by

$$< S_i >= Z^{-1}\mathrm{Tr}[\mathcal{S}(FG)^{\frac{N}{2}}]. \tag{18}$$

2.1. When j-i is even

In this case, we write (17) as

$$\begin{aligned} < S_i S_j >= Z^{-1}\mathrm{Tr}[\quad & DD^{-1}\mathcal{S}D\,\underbrace{D^{-1}FGD...D^{-1}FGD}\,D^{-1}\mathcal{S}D \\ & \underbrace{D^{-1}FGD...D^{-1}FGD}\,D^{-1}], \end{aligned} \tag{19}$$

where the first underbrace contains $\alpha/2$ terms of $D^{-1}FGD$ and the second one contains $(N-\alpha)/2$ terms. To simplify things further, we define S_1, S_2, S_3 and S_4 such that

$$D^{-1}SD = \begin{pmatrix} \mathcal{S}_1 & \mathcal{S}_2 \\ \mathcal{S}_3 & \mathcal{S}_4 \end{pmatrix}. \tag{20}$$

More explicitly,

$$\begin{aligned} \mathcal{S}_1 &= \frac{-A(-1+B^4)\sqrt{C}}{\sqrt{A^2C+4B^2C+4B^6C+A^2B^8C+B^4(4-2A^2C+4C^2)}}, \\ \mathcal{S}_2 &= \frac{-A(-1+B^4)\sqrt{C}-\sqrt{A^2C+4B^2C+4B^6C+A^2B^8C+B^4(4-2A^2C+4C^2)}}{\sqrt{A^2C+4B^2C+4B^6C+A^2B^8C+B^4(4-2A^2C+4C^2)}}, \end{aligned}$$

$$\mathcal{S}_3 = \frac{A(-1+B^4)\sqrt{C} - \sqrt{A^2C+4B^2C+4B^6C+A^2B^8C+B^4(4-2A^2C+4C^2)}}{\sqrt{A^2C+4B^2C+4B^6C+A^2B^8C+B^4(4-2A^2C+4C^2)}},$$

$$\mathcal{S}_4 = \frac{A(-1+B^4)\sqrt{C}}{\sqrt{A^2C+4B^2C+4B^6C+A^2B^8C+B^4(4-2A^2C+4C^2)}}. \tag{21}$$

Then it follows that

$$< S_iS_j >= Z^{-1}\mathrm{Tr}\Big[D^{-1}\mathcal{S}D\begin{pmatrix}\lambda_1^{\frac{\alpha}{2}} & 0\\ 0 & \lambda_2^{\frac{\alpha}{2}}\end{pmatrix}D^{-1}\mathcal{S}D\begin{pmatrix}\lambda_1^{\frac{N-\alpha}{2}} & 0\\ 0 & \lambda_2^{\frac{N-\alpha}{2}}\end{pmatrix}\Big]. \tag{22}$$

Now using (20), after carrying out the matrix multiplications we reach at

$$< S_iS_j >= Z^{-1}\mathrm{Tr}\Big[\begin{pmatrix}\mathcal{S}_1^2\lambda_1^{\frac{N}{2}}+\mathcal{S}_2\mathcal{S}_3\lambda_1^{\frac{N-\alpha}{2}}\lambda_2^{\frac{\alpha}{2}} & \mathcal{S}_1\mathcal{S}_2\lambda_1^{\frac{\alpha}{2}}\lambda_2^{\frac{N-\alpha}{2}}+\mathcal{S}_2\mathcal{S}_4\lambda_2^{\frac{N}{2}}\\ \mathcal{S}_1\mathcal{S}_3\lambda_1^{\frac{N}{2}}+\mathcal{S}_3\mathcal{S}_4\lambda_2^{\frac{\alpha}{2}}\lambda_1^{\frac{N-\alpha}{2}} & \mathcal{S}_2\mathcal{S}_3\lambda_1^{\frac{\alpha}{2}}\lambda_2^{\frac{N-\alpha}{2}}+\mathcal{S}_4^2\lambda_2^{\frac{N}{2}}\end{pmatrix}\Big]. \tag{23}$$

Taking the trace, we get,

$$< S_iS_j >= Z^{-1}\mathcal{S}_1^2\lambda_1^{\frac{N}{2}}+\mathcal{S}_2\mathcal{S}_3\lambda_1^{\frac{N-\alpha}{2}}\lambda_2^{\frac{\alpha}{2}}+\mathcal{S}_2\mathcal{S}_3\lambda_1^{\frac{\alpha}{2}}\lambda_2^{\frac{N-\alpha}{2}}+\mathcal{S}_4^2\lambda_2^{\frac{N}{2}}. \tag{24}$$

Now in the thermodynamic limit (with $N\to\infty$), using the fact that $\lambda_2>\lambda_1$, we get

$$< S_iS_j > = \frac{1}{\lambda_2^{\frac{N}{2}}}\Big[\mathcal{S}_4^2\lambda_2^{\frac{N}{2}}+\mathcal{S}_2\mathcal{S}_3\Big(\frac{\lambda_1}{\lambda_2}\Big)^{\frac{\alpha}{2}}\lambda_2^{\frac{N}{2}}\Big] \tag{25}$$

$$= \mathcal{S}_4^2+\mathcal{S}_2\mathcal{S}_3\Big(\frac{\lambda_1}{\lambda_2}\Big)^{\frac{\alpha}{2}}. \tag{26}$$

Further, using (18), we therefore have

$$< S_iS_j > - < S_i >< S_j >= \mathcal{S}_2\mathcal{S}_3\Big(\frac{\lambda_1}{\lambda_2}\Big)^{\frac{\alpha}{2}}. \tag{27}$$

2.2. When $j-i$ is odd

In the case when $j-i$ is odd, the correlator takes the form:

$$< S_iS_j >= Z^{-1}\mathrm{Tr}[\quad DD^{-1}\mathcal{S}D\underbrace{D^{-1}FGD...D^{-1}FGD}D^{-1}F\mathcal{S}GD$$
$$\underbrace{D^{-1}FGD...D^{-1}FGD}D^{-1}], \tag{28}$$

where the first underbrace contains $(j-i-1)/2$ terms of $D^{-1}FGD$ and the one in the second underbrace has $(N-(j-i-1)-2)/2$ terms. Here also we will continue to write $j-i$ as α. Now, denoting

$$D^{-1}F\mathcal{S}GD = \begin{pmatrix}x_1 & x_2\\ x_3 & x_4\end{pmatrix} \tag{29}$$

we can write the correlator as

$$\begin{aligned} < S_i S_j > &= Z^{-1}\mathrm{Tr}\Big[D^{-1}\mathcal{S}D \begin{pmatrix} \lambda_1^{\frac{\alpha-1}{2}} & 0 \\ 0 & \lambda_2^{\frac{\alpha-1}{2}} \end{pmatrix} [D^{-1}F\mathcal{S}GD] \begin{pmatrix} \lambda_1^{\frac{N-\alpha-1}{2}} & 0 \\ 0 & \lambda_2^{\frac{N-\alpha-1}{2}} \end{pmatrix}\Big] \\ &= Z^{-1}\mathrm{Tr}\Big[D^{-1}\mathcal{S}D \begin{pmatrix} \lambda_1^{\frac{\alpha-1}{2}} & 0 \\ 0 & \lambda_2^{\frac{\alpha-1}{2}} \end{pmatrix} \begin{pmatrix} x_1 & x_2 \\ x_3 & x_4 \end{pmatrix} \begin{pmatrix} \lambda_1^{\frac{N-\alpha-1}{2}} & 0 \\ 0 & \lambda_2^{\frac{N-\alpha-1}{2}} \end{pmatrix}\Big] \end{aligned} \tag{30}$$

Note that since $\mathcal{S}, F, G$ and D are explicitly known, x_1, x_2, x_3, x_4 are calculable quantities. We can now progress as before to calculate (30). Since the manipulations are simple, we will skip the details. The final result, in the thermodynamic limit, turns out to be:

$$< S_i S_j >= \frac{1}{\lambda_2}\Big[\mathcal{S}_3 x_4 + \Big(\frac{\lambda_1}{\lambda_2}\Big)^{\frac{\alpha-1}{2}} \mathcal{S}_4 x_2\Big], \tag{31}$$

where $\mathcal{S}_3$ and $\mathcal{S}_4$ are given in (21). Further,

$$< S_i S_j > - < S_i >< S_j >= \frac{1}{\lambda_2}\Big(\frac{\lambda_1}{\lambda_2}\Big)^{\frac{\alpha-1}{2}} \mathcal{S}_4 x_2. \tag{32}$$

From (27) and (32), we see that the correlation dies off with the distance between the spins α since $\lambda_2 > \lambda_1$. However, it follows from (9) that if A, B, C satisfy

$$A^2C + 4B^2C + 4B^6C + A^2B^8C + B^4(4 - 2A^2C + 4C^2) = 0, \tag{33}$$

then $\lambda_2 = \lambda_1$. In this special case, correlation no longer falls with the distance (between the spins). This represents the appearence of long range correlation in the system. This critical point is normally described by introducing a *correlation length* ξ as

$$\xi = \frac{1}{\ln(\frac{\lambda_2}{\lambda_1})}. \tag{34}$$

This diverges when $\lambda_2 = \lambda_1$.

3. DISCUSSIONS

We have shown that the spin-spin correlator for the dimerized Ising chain can be explicitly calculated. From the divergence of the correlation lenth, we have isolated the critical point of the system. Are the higher point correlators calculable? We leave this for future.

Note added:

After completing the work, we were informed by Goutam Tripathy that these results were presented in [4]. We thank him for bringing this paper into our notice.

Acknowledgements

This work is done under the supervision of Sudipta Mukherji, Institute of Physics, Bhubaneswar. We thank Somen Bhattacharjee for his instructive comments on the draft.

References

[1] R. J. Baxter, Exactly solved models in statistical mechanics, Academic Press, 1982, pp 32 - 38.

[2] K.A. Penson, A. Holtz and K.H. Bennemann, Theory of the Peierls transition in coupled electron and classical spin systems, Phys. Rev. B13, 433, 1976.

[3] C. E. Zaspel, A tricritical point in the dimerized Ising chain phase diagram, Am.J.Phys. 58 (10), 992, 1990.

[4] M. Mijatovic and S. Milosevic, Equal time correlation functions of the dimerized Ising chain with next-nearest neighbour interactions, Phys. Lett. A, 79, 196, 1980.

P R A Y A S
Students' Journal
of Physics

An effective mass theory for nano-heterostructure

Shilpi Singh[1], Praveen Pathak[2*] and Vijay A. Singh[3]
[1]Centre for Excellence in Basic Sciences Health Centre, University of Mumbai, Vidhyanagari Campus, Mumbai - 400098
[2]Homi Bhabha Centre for Science Education (TIFR), V. N. Purav Marg, Mankhurd, Mumbai-400088, India
[3]Homi Bhabha Centre for Science Education (TIFR), V. N. Purav Marg, Mankhurd, Mumbai-400088, India

Communicated by: A.M. Srivastava

1. INTRODUCTION

The finite 1-D potential well is an elementary textbook problem in quantum mechanics. Quantum mechanics textbooks describe the graphical solution for the eigen-values without actually obtaining them. [1–4, 6] Some books do go a step further and obtain an exact condition for total number of bound states in the well. The treatment often leaves the student dissatisfied. The purpose of this work is to obtain an analytical solution when the potential is deep and also complementary in the limit of shallow well. We also carry out numerical calculation to validate our results.

The graphical solution of the problem is obtained using continuity condition across the boundary for the wavefunction and its derivative. We adopt a more general approach in which we take the mass of the particle inside the well (m_i) which is different from mass outside the well (m_o) and was discussed by Ben-Daniel and Duke in the context of semiconductors. [5] A relevant parameter therefore is the mass discontinuity ratio $\beta = m_i/m_o$. In Sec. .2. we obtain the result using Ben-Daniel Duke boundary condition (BDD). The standard textbook model is then simply a special case of our more general approach. Note that our treatment is relevant in the context of discussion of quantum wells and heterostructures. [6]

We exploit our methodology for the case of deep and shallow well in Sec. .3.. The energy states of a particle in finite potential well (V_0) of length L is dependent on parameters β, V_o and L. We define a dimensionless parameter $\epsilon = \left(2m_iE_n/\hbar^2\right)^{1/2}L/2$ where E_n is the nth eigenstate of the particle. The analytical solution is carried out using the approximation namely $\tan(\epsilon) \approx \epsilon$. For the

*praveen@hbcse.tifr.res.in

deep well case the approximation used in Sec. 3. 3.1. is no longer valid due to large ϵ. We define another dimensionless parameter $\epsilon_h = \pi/2 - (2m_i E_n/\hbar^2)^{1/2} L/2$. The analytical solution is carried out using the approximation $\tan(\frac{\pi}{2} - \epsilon_h) \approx 1/\epsilon_h$. Section .4. constitutes the discussion.

2. BASIC THEORY IN ONE DIMENSION

We consider an one dimensional finite potential well (V_0) of length L as given in Fig. (1) with the effective mass (m^*) of the particle given by

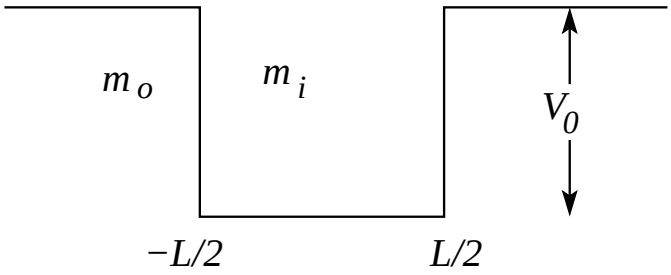

Figure 1. The finite well of extent $-L/2 < x < L/2$ and height V_0.

$$\begin{aligned} m^*(x) = \quad & m_i \; |x| < L/2 \\ & m_o \; |x| > L/2 \end{aligned} \tag{1}$$

where m_i and m_o are constants. A relevant parameter therefore is the mass discontinuity ratio $\beta = m_i/m_o$. An electron in this well is described using effective mass theory by the Hamiltonian

$$H \;=\; -\frac{\hbar^2}{2}\frac{d}{dx}\left[\frac{1}{m^*(x)}\frac{d}{dx}\right] + V(x) \tag{2}$$

The first term in the right-hand side of Eq. (2) is the appropriate Hermitian kinetic energy for a position dependent mass and was purposed by Ben-Daniel and Duke. The second term is the potential energy given by

$$\begin{aligned} V(x) = \quad & 0 \; |x| \leq L/2 \\ & V_o \; |x| > L/2 \end{aligned} \tag{3}$$

where V_0 is barrier height typically between 1 eV and 10 eV.
A typical solutions for the wave function for $|x| \leq L/2$ are

$$\Psi_n(x) = A_I \cos(k_{n,in} x) \qquad \text{for even states} \tag{4}$$

$$\Psi_n(x) = A_I \sin(k_{n,in} x) \qquad \text{for odd states} \tag{5}$$

While for $|x| > L/2$ the solution is

$$\Psi_n(x) = B_I e^{-k_{n,out}x} \tag{6}$$

where the wave vectors are

$$k_{n,in} = \sqrt{\frac{2m_i E_n}{\hbar^2}} \tag{7}$$

and

$$k_{n,out} = \sqrt{\frac{2m_o(V_o - E_n)}{\hbar^2}} \tag{8}$$

Here A_I and B_I are normalisation constants. E_n is the energy of the n^{th} eigen-state. Usual boundary condition demands that the wavefunction is continuous at $x = \pm L/2$ i.e.

$$\Psi_n|_{x\to(L/2)^-} = \Psi_n|_{x\to(L/2)^+} \tag{9}$$

and

$$\frac{1}{m_i}\frac{d\Psi_n}{dx}\bigg|_{x\to(L/2)^-} = \frac{1}{m_o}\frac{d\Psi_n}{dx}\bigg|_{x\to(L/2)^+} \tag{10}$$

The above condition is called the Ben-Daniel-Duke boundary condition (BDD). The standard derivative condition gets modified since the mass changes across the barrier. In terms of parameter β Eq. (10) can be rewritten as

$$\frac{d\Psi_n}{dx}\bigg|_{x\to(L/2)^-} = \beta\,\frac{d\Psi_n}{dx}\bigg|_{x\to(L/2)^+} \tag{11}$$

If we take β to 1, above condition returns in standard boundary condition of continuity in derivatives which is found in textbooks. Note that the Ben-Daniel Duke boundary condition is relevant in the study of low-dimensional semiconductor structures. Using Eqs. (4), (5) and (6) in boundary conditions, the eigenvalue conditions for even and odd states are given as

$$k_{n,in}\tan\left(k_{n,in}\frac{L}{2}\right) = \beta k_{n,out} \qquad \text{for even states} \tag{12}$$

$$k_{n,in}\cot\left(k_{n,in}\frac{L}{2}\right) = -\beta k_{n,out} \qquad \text{for odd states} \tag{13}$$

The condition for existence of (N +1) bound states is

$$\frac{N}{2}\pi \leq \sqrt{\frac{\beta m_o V_o L^2}{2\hbar^2}} < \frac{N+1}{2}\pi \tag{14}$$

The Eq. (14) is similar to the one encountered in textbooks. The presence of $\sqrt{\beta}$ explains the reduction in number of bounded states by a factor of 3 for $\beta = 0.1$.

3. ASYMPTOTIC ANALYSIS

3.1. Shallow Well

In the one-dimensional case the eigenvalue condition for the ground state is given by Eq. (12). For low V_o , the solution of Eq. (12) for the ground state may be approximated as

$$\frac{k_{1,in}L}{2} = \epsilon \tag{15}$$

where ϵ is a small positive quantity. If we substitute Eq. (15) in Eq. (12) , we get

$$\epsilon = \sqrt{\beta k_{1,out}\frac{L}{2}} \tag{16}$$

Substituting Eq. (16) in Eq. (15) yields

$$\frac{k_{1,in}L}{2} = \sqrt{\beta k_{1,out}\frac{L}{2}} \tag{17}$$

which results in the expression for ground state energy E_1,

$$E_1 = 2V_o\frac{\sqrt{1+\sigma_l}-1}{\sigma_l} \tag{18}$$

where

$$\sigma_l = \frac{2m_0V_oL^2}{\hbar^2} \tag{19}$$

The expression obtained is independent of β.

3.2. Deep Well

For large V_o , the solution of Eq. (12) for the ground state may be approximated as

$$\frac{k_{1,in}L}{2} = \frac{\pi}{2} - \epsilon_h \tag{20}$$

where ϵ_h is a small positive quantity. If we substitute Eq. (20) in Eq. (12) , we find

$$\epsilon_h = \frac{\pi}{\beta k_{1,out}L + 2} \tag{21}$$

We introduce the dimensionless parameter σ as

$$\sigma = \beta^2\frac{2m_oV_o}{\hbar^2}L^2 \tag{22}$$

and obtain

$$\epsilon_h \approx \frac{\pi}{\sqrt{\sigma}+2} \tag{23}$$

We substitute Eq. (23) in Eq. (20) to obtain

$$k_{1,in} = \frac{\pi}{2}\left[1 - \frac{2}{\sqrt{\sigma}+2}\right] \tag{24}$$

which yields an asymptotic expression for ground state energy E_1 ,

$$E_1 = \frac{\pi^2\hbar^2}{2m_iL^2}\left[1 - \frac{2}{\sqrt{\sigma}+2}\right]^2 \tag{25}$$

The second term in square bracket is the correction to infinite barrier.

4. RESULTS

4.1. SHALLOW WELL

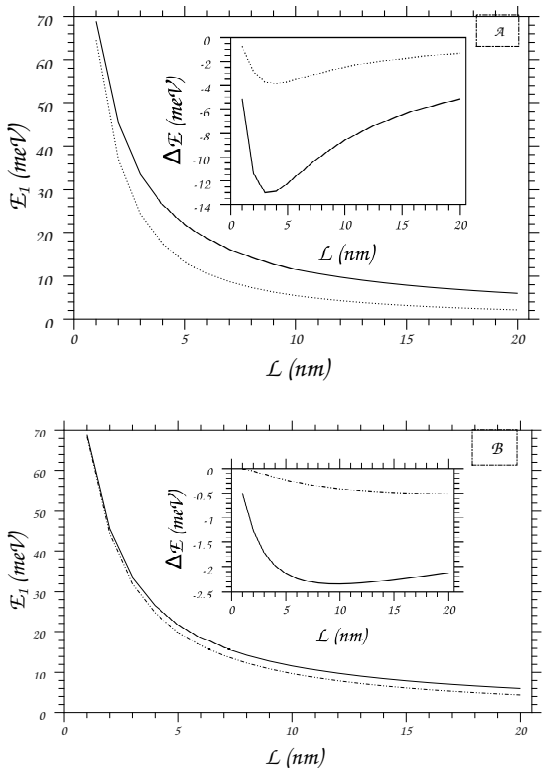

Figure 2. The variation in ground state energy (E_1) with L for well parameter $V_0 = 100$ meV and (A) $\beta = 1$, (B) $\beta = .1$. The solid (dashed) line represents the first (higher) order approximation to E_1 discussed in the text. The inset shows the difference ΔE between the approximation and the exact results.

The formalism in Sec. III yields the following results for potential well having barrier height $V_o = 100$ meV , 10 meV and 5 meV.

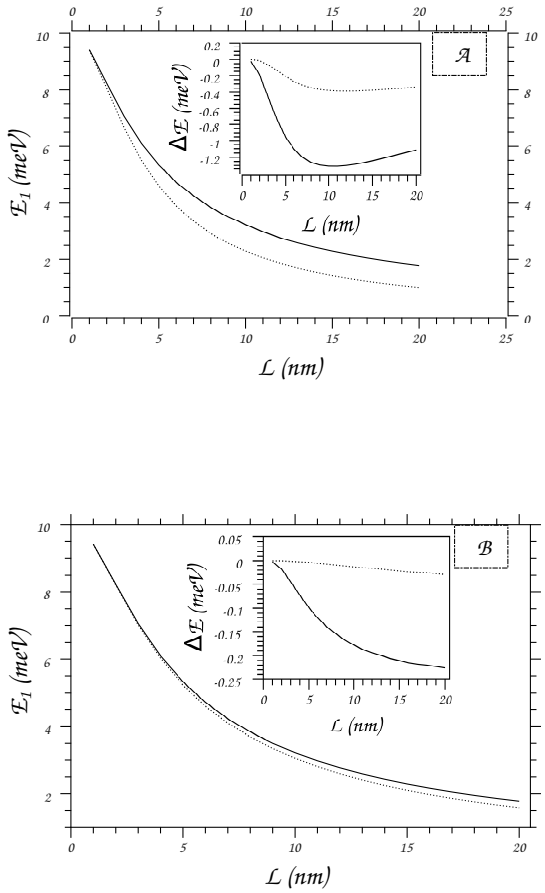

Figure 3. The variation in ground state energy (E_1) with L for well parameter $V_0 = 10$ meV and (A) $\beta = 1$, (B) $\beta = .1$. The solid (dashed) line represents the first (higher) order approximation to E_1 discussed in the text. The inset shows the difference ΔE between the approximation and the exact results.

In the curves shown above, the term ΔE is calculated by subtracting the ground state energy E_1 obtained using approximation numerically from the E_1 obtained from Eq. (12). Ground state energy (E_1) is obtained using solution of first order approximation. The result shows that the approximation works better for small (large) β in case of shallow (deep) well. That is what we expected since the approximation is based on small (large) σ which itself is a function of β. Using Eq. (14) one can calculate number of bound state which are given in Table 1.

Table 1. Number of bound states for various values of V_0 and β.

$V_0(meV)$	β	L (nm)	Number of bound states
5	.1	1	1
5	.1	20	1
5	1	1	1
5	1	20	3
10	.1	1	1
10	.1	20	2
10	1	1	1
10	1	20	4
100	.1	1	1
100	.1	20	2
100	1	1	1
100	1	20	11

Acknowledgement

This work was supported by the National Initiative on Undergraduate Science (NIUS) under taken by Homi Bhabha Centre for Science Education (HBCSE-TIFR), Mumbai, India.

References

[1] E. Merzbacher, Quantum Mechanics, John Wiley and Sons, New York (1970).

[2] A. Beiser, Concepts of Modern Physics, McGraw-Hill, New York (2002).

[3] R.W. Robinett, Quantum Mechanics, Oxford University Press, New York (2006).

[4] L. Schiff, Quantum Mechanics, McGraw-Hill, Singapore (1968).

[5] D.J. BenDaniel and C.B. Duke, Space-Charge Effects on Electron Tunneling, Phys. Rev., Vol.152, No. 2, p-683 (1966)

[6] C. Weisbuch and B. Vinter, Quantum Semiconductor Structures, Academic Press, San Diego (1991).

P R A Y A S
Students' Journal
of Physics

Physics behind supercavitation and the underlying forces in a supercavitating vehicle*

Ravi Prakash Ranjan
IInd yr., Intg. MS, IISER - Kolkata, Mohanpur- 741252, Nadia, West Bengal, India

Abstract. The velocity of conventional underwater vehicles is limited by the drag produced by skin friction i.e., interaction of liquid with the vehicle surface. Traditional ways of improving propulsion and streamlining the vehicle does not lead to significant speed increase. However, if surface area of the vehicle in contact with the liquid phase gets reduced, then skin friction can be eliminated considerably. Supercavitation helps in exactly doing that. It can drastically reduce the wetted surface area by enveloping the vehicle with gaseous water vapor, leading to an order of magnitude reduction in drag, if the body is shaped properly. Drag is localized at the nose of the vehicle, where a cavitator generates a cavity that completely envelops the body, at the fins and on the vehicle after-body. Here, we are focussing on the physics behind supercavitation and the forces acting on supercavitating vehicles.

Keywords. supercavitation, rotation tensor, penetration distance.

Communicated by: Prasanta K. Panigrahi

1. INTRODUCTION TO SUPERCAVITATION

Cavitation is the breaking of the liquid medium under excessive stress, which is a fundamental property of a liquid, since it cannot withstand the same beyond a critical point. In our discussions we will be concerned with cavitation in water. As it is known, water is a practically incompressible medium having properties, weakly changing under pressure. When the pressure in liquid reduces to a value lower than the saturated vapor pressure, owing to action of extending stresses, discontinuities in the form of bubbles, foils and cavities occur, which are filled by water vapor.

When a cavity is formed, vapor evaporates into the cavity from the surrounding medium, thus the cavity is not a perfect vacuum, but has a relatively low gas pressure. Such a low pressure cavitation bubble in liquid begins to collapse, due to higher pressure of the surrounding medium. As the bubble collapses, the pressure and temperature of the vapor within also increases. The bubble

*A Review

eventually collapses to a fraction of its original size, at which point the gas within dissipates into the surrounding liquid via a violent mechanism. A huge amount of energy in the form of acoustic shock waves are released leading to a very high temperature at this point. Due to the erosion made by the collapse of cavity bubble, cavitation is undesirable for propellers and turbine blades, as it decreases the efficiency of underwater vehicles.

Supercavitation uses the phenomenon of cavitation in a large and sustained manner. Generally supercavitating objects have sharp flat leading edges on a streamlined, hydrodynamic or aerodynamic shape. When the object is travelling through water at high speeds, the nose deflects the water so fast that the pressure of the fluid at the back of the nose starts dropping rapidly. The water vaporizes when the pressure drops below the vapor pressure. The pressure of the surrounding water forces the bubble to collapse, which takes time and thus the nose opens an extended bubble of water behind it. Given a sufficient speed, the cavity can extend itself to cover the entire body. This phenomenon is termed as 'supercavitation'. Fig.1 shows the configuration of a supercavitating vehicle (SCV).

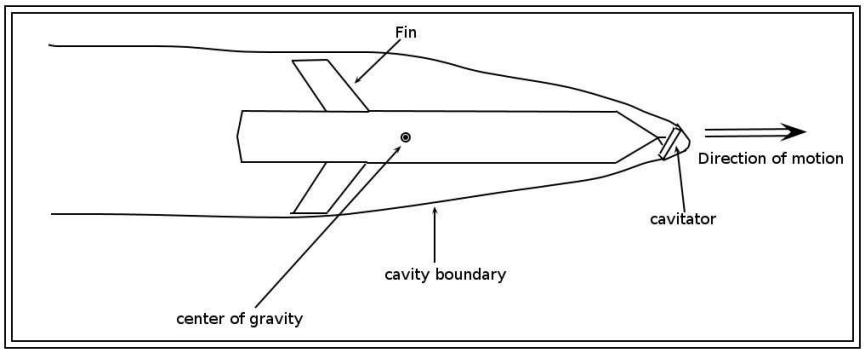

Figure 1. Configuration of a supercavitating vehicle.

2. PHYSICS BEHIND SUPERCAVITATION

To develop a deeper insight into the supercavitation phenomenon, we start from cavitation. As stated above, when there is excessive stress or the pressure of the flowing fluid decreases to less than that of saturated vapor pressure, the breaking of liquid medium occurs. In order to solve the problem of excessive stresses, we need a threshold of stress, beyond which the liquid cohesion is no longer ensured. The threshold should be determined from physical consideration at microscopic scale. For explicitness, we consider a liquid bubble of radius R inside a flowing liquid. Within the bubble the vapor pressure is P_v, P_g is partial pressure of the gas and outside external pressure is denoted by P. The condition for the mechanical equilibrium can be written in the form,

$$P_v + P_g = P + \frac{2S}{R},$$

where S is the surface tension of the bubble.

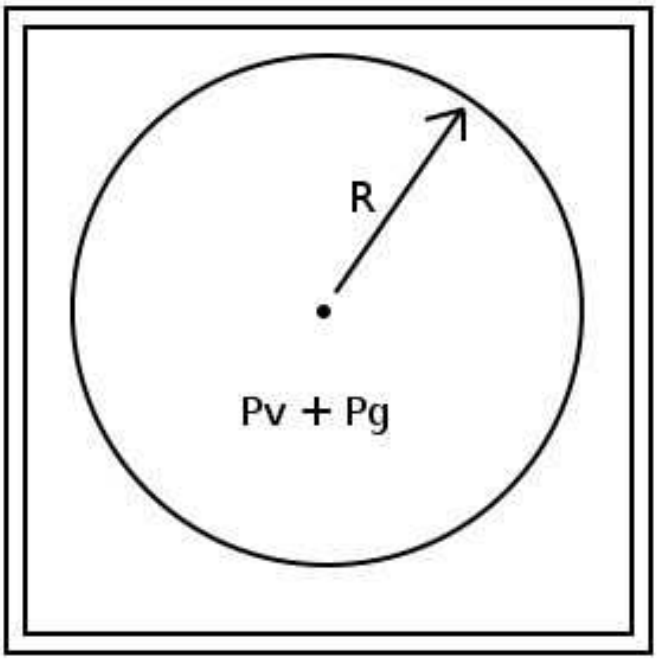

Figure 2. A cavitation bubble in mechanical equilibrium.

The condition for the bubble to grow is given by:

$$P_v + P_g > P + \frac{2S}{R}.$$

When the flowing fluid has a relatively high velocity, P_v starts decreasing which follows from the Bernoulli's equation, $P + \rho gh + \frac{1}{2}\rho V^2 = constant$. Soon the condition arises, when P_v reaches below its saturated vapor pressure value wherein a cavity is formed.

The physical process for the formation of cavity is similar to boiling. The major difference between them is the two thermodynamic paths, which precede the formation of vapor. Boiling occurs when the local vapor pressure of the liquid rises above its local ambient pressure and sufficient energy is present to cause the phase change to a gas. Cavitation inception occurs, when the local pressure falls sufficiently below the saturated vapor pressure. However, in some cases the heat transfer needed for vaporization is such that the phase change occurs at temperature T_f', lower than the ambient liquid temperature T_f. The temperature difference $T_f - T_f'$ is known as thermal delay of cavitation. This is illustrated in Fig. 3.

A supercavitating vehicle has a cavitator attached in its front part. When this vehicle runs at very high speed in water, the cavitator deflects the water outward so fast that the pressure of the fluid in the rear end of the cavitator drops suddenly. Now the water starts vaporizing and the pressure drops below the saturated vapor pressure. The pressure of surrounding water forces the bubble to collapse but water pressure vanishes slowly and it takes time to collapse on the wall of the resulting cavity,

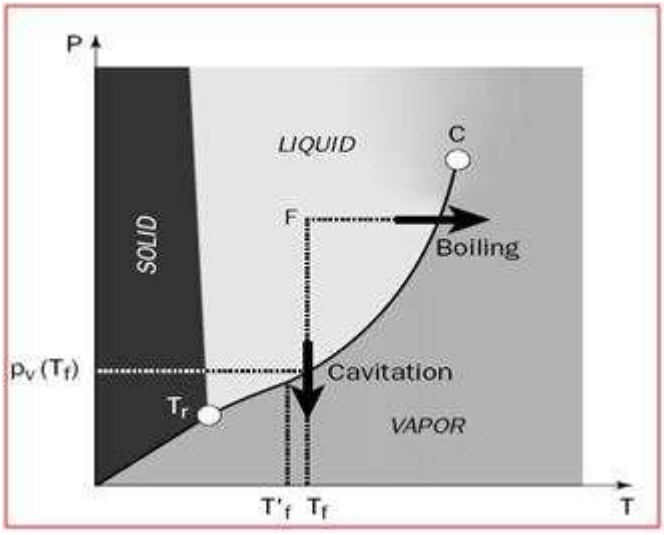

Figure 3. Diagram showing the phase changes as a function pressure and temperature, with emphasis on the point where the cavitation occurs.

hence an extended bubble of water vapor opens at the nose. Owing to streamlined, hydrodynamic and aerodynamic shape of the supercavitating object and the typical shape of the cavitator, the bubble gets extended further. If the speed is sufficient or some gas is injected into the partially developed cavity then it gets extended to cover the entire body. So, supercavitation can provide significant benefit for drag reduction by maintaining a stable, single vaporous bubble around the vehicle resulting in extended velocity and a range of other underwater applications. Now we will discuss the quantitative description of the dynamics of a supercavitating vehicle.

2.1 Cavitation number

Cavitation number (σ) is one of the important supercavitating flow parameters. It is defined as:

$$\sigma = \frac{(P_\infty - P_c)}{(\frac{1}{2}\rho V^2)}$$

where ρ is the density of the fluid, P_∞ is the ambient pressure (pressure at chosen reference point in the surrounding medium), P_c is the pressure inside the cavity and V is the velocity of the vehicle. Cavitation number captures the tendency for the cavitation to occur in a flow, hence it is a significant quantity governing the cavity dimensions.

Lower the cavitation number, more stable is the supercavity because for σ to be less, V should be high so that the bubble can surround the cavity completely. Cavitation number is also related to the drag experienced by the vehicle and flow angle of attack of the vehicle:

$$C_D(\sigma, \alpha_c) = C_{D0}(1 + \sigma)cos^2\alpha_c$$

where $C_D(\sigma, \alpha_c)$ is the drag when cavitation number is σ and the angle of attack is α and C_{D0} is the drag coefficient at zero angle of attack, and it's value can be determined experimentally.

3. CALCULATIONS OF FORCES ON SUPERCAVITATING VEHICLES

To calculate the forces, we need to understand the configuration of supercavitating vehicle. Here we have considered control surfaces, cavitator and fins. The figure below presents the configuration of a supercavitating vehicle with the applied forces.

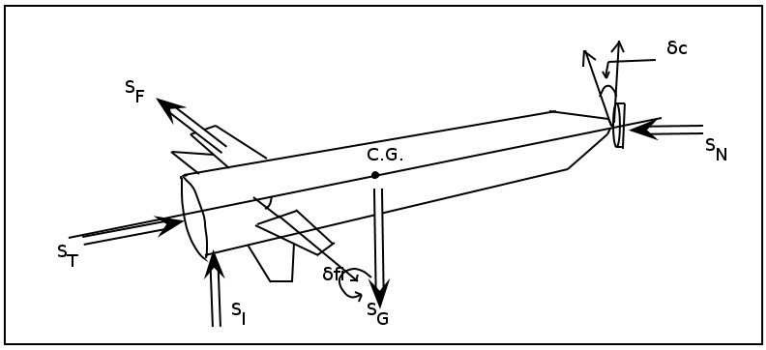

Figure 4. Configuration of a supercavitating vehicle with applied forces.

The body is acted upon by the system of forces corresponding to the interaction of the vehicle control surfaces with the cavity boundaries.

In the above figure, S_G = force due to gravity; S_N = force on nose (cavitator); S_F = force on a fin; S_T = thrust ; S_I = contact force due to interaction of vehicle with the cavity; δ_{Fi} & δ_C are control deflection angles of the fins and the cavitator respectively.

For a given SCV its mass, length, cavitator diameter are known and angle of attacks and control angles can be measured using angle of attack sensor or angle of slide slip sensor, which are attached on the front part of SCV. Forces are to be calulated in terms of known parameters. We have attached here one frame of reference to the body, which is non inertial and another outside the body which is an inertial one .This has been done keeping in mind the Euler equations of motion for a rotating rigid body.

The first reference frame $F_{P\beta}$ is a body fixed reference frame with origin P. A reference inertial frame $F_{o\varepsilon}$ is centered at point O outside the SCV.

Let S be the net force acting on the particle, then

$$S = S_N + S_T + S_G + S_I + \Sigma S_{fi},$$

here S_{fi} is the force exerted on the i-th fin.

Considering the moments, we calculate net moment M as,

$$M = r_{PT} \times S_T + r_{PN} \times S_N + (m_I + r_{PI} \times S_I) + r_{PG} \times S_G + (m_{fi} + r_{Pfi} \times S_{fi}).$$

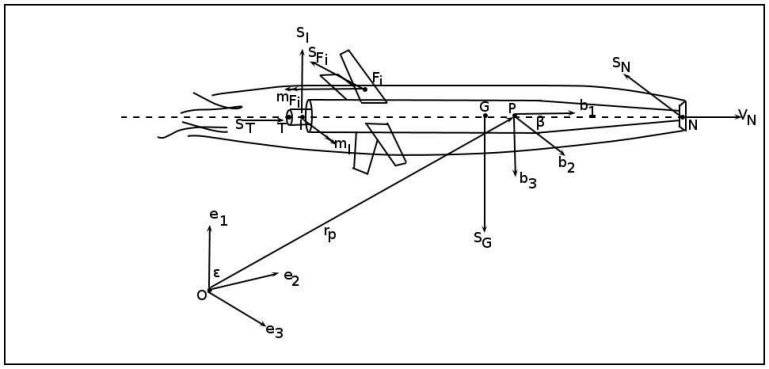

Figure 5. Different frames of references for the SCV.

All position vectors have been measured from the reference frame $F_{P\beta}$.

Bold lowercase letters indicate vectors while bold uppercase letters indicate matrices or tensors, also $(.)^{\beta}$ denotes the components in the triad. If R is the rotation tensor that brings triad I into triad β ,then the component of a generic vector A in the two triad are related as A^I=R^I A^{β}.

We now focus on the calculation of forces. There are five forces, so we calculate each, starting with the simplest one, gravity.

Force due to gravity

The force due to gravity acts downwards and in the reference $F_{o\varepsilon}$and it is given by,

$$S_G = -mge_3$$

Since m and g are known so S_G can be deduced. Here $e_3$is a unit vector in the triad ε.

3.1 Thrust calculations

Thrust depends upon the type of engine used for the given SCV. If a rocket engine is used, then the thrust S_T is given by a common formula, replacing atmospheric pressure by cavitation pressure.

$$S_T = V_e \frac{dm}{dt} + (P_e - P_c)$$

V_e being exhaust velocity, $\frac{dm}{dt}$ is the mass flow rate, P_e and A_e are exit pressure and area respectively and P_c is cavitation pressure.

Instead if one considers an airplane engine, then the calculations are different. For this purpose we focus on the propeller disk as in the diagram below. Here P_0 is the pressure inside the cavity, V_0 is the velocity of SCV, $V_e$is the exit/exhaust velocity, ρ is the density of the fluid. We will apply Bernoulli's equation on both sides of the propeller disk and calculate the change in pressure across the propeller disk, multiplication with area yields the thrust value.

If the change in propeller disk is ΔP, then

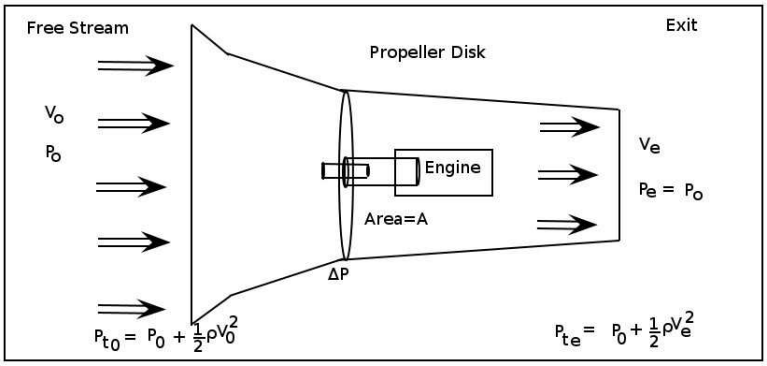

Figure 6. Thrust calculations using an airplane engine.

$$\Delta P = Pt_e - Pt_0$$

$$= (P_0 + \frac{1}{2}\rho V_e^2) - (P_0 + \frac{1}{2}\rho V_0^2)$$

$$= \frac{1}{2}\rho(V_e^2 - V_0^2)$$

Thrust is given by,

$$S_T = A\Delta P$$

Hence

$$S_T = \frac{1}{2}\rho A(V_e^2 - V_0^2)$$

All the quantities in the right hand side are known , so S_T can be calculated.

3.2 Forces calculations on the cavitator

Apart from cavity generation, cavitator helps in providing the lift force. To achieve optimal orientation of the cavity with respect to the vehicle, during turning maneuvers requires this angle to be variable and controllable. The force generated on the cavitator through its interaction with water can be used for controlling the vehicle by orienting it at a proper angle. The hydrodynamic force acting on a circular cavitator can be conveniently expressed in terms of reference frame $F_{N,N}$ located at the cavitator center N and with a triad unit vectors attached to it.

$$N = (n_1, n_2, n_3) \qquad (see\ fig.\ 7)$$

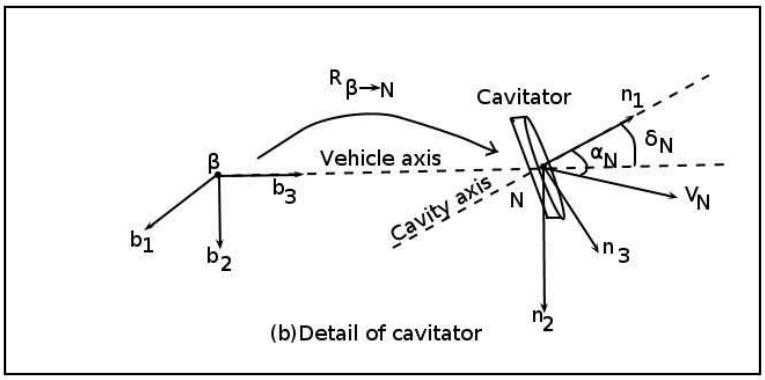

Figure 7. Cavitator reference frame.

Unit vector $n_1$is perpendicular to the disc surface. Its orientation with respect to the vehicle axis b_1 is defined by control angle δ_N, so that the corresponding components of in the body fixed triad β, labeled as n_1^β , are:

$$n_1 = (cos\delta_N, 0, -sin\delta_N)^T$$

Unit vector n_2 is perpendicular to plane formed by V_N and n_1, hence,

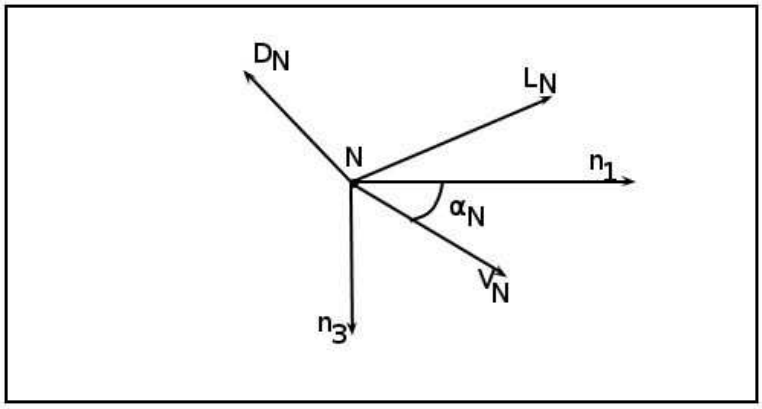

Figure 8. Lift and drag components in the V_N and n_1 plane.

$$n_2 = \frac{V_N \times n_1}{\|V_N \times n_1\|}$$

and unit vector n_3 is given by $n_1 \times n_2$.

The components of these unit vectors in the triad β give rise to a rotation tensor $R_{\beta\to N}$ that rotates β into triad N.

If V_N^β denotes the components of the cavitator velocity in the β triad, the components of the same vector in the cavitator triad N are,

$$V_N^N = R_{\beta\to N}^{\beta} V_N^{\beta} = (U_N^N, 0, W_N^N)^T$$

The cavitator angle α_N of attack is measured in the V_N, n_1 plane (Fig. 7) and it is computed as

$$tan\alpha_N = \frac{W_N^N}{U_N^N}$$

In the V_N,$n_1$plane, the hydrodynamic force acting on the cavitator can be decomposed into lift and drag components:

$$L_N = \frac{1}{2}\rho V_N^2 A_N C_D(\sigma, 0) sin\alpha_N cos\alpha_N$$

and

$$D_N = \frac{1}{2}\rho V_N^2 A_N C_D(\sigma, 0) cos^2\alpha_N$$

and therefore

$$S_N^N = (L_N sin\alpha_N - D_N cos\alpha_N, 0, \ -L_N cos\alpha_N - D_N sin\alpha_N).$$

This can be transformed to triad β as

$$S_N^{\beta} = R_{\beta\to N}^{\beta} S_N^N$$

Before we describe the calculation of other two forces, we need to understand the penetration distance.

1 Penetration distance

It is the distance penetrated by fins or tail, when they interact with cavity boundaries. The fin penetration distance D_{fi} is calculated in terms of the dimensions of the cavity sustained by the vehicle velocity. The distance of the fin from the cavity axis is given by

$$Dfi = \|r_{Nfi}\| sin\theta,$$

where θ is angle between the cavity axis and distance vector. The penetration distance of the i-th fin is approximated as:

$$D_{fi} = D_{ci} - r_c(\xi_0),$$

where $r_c(\xi_0)$ is radius of the cavity at $\xi = \|r_{nfi} cos\theta\|$

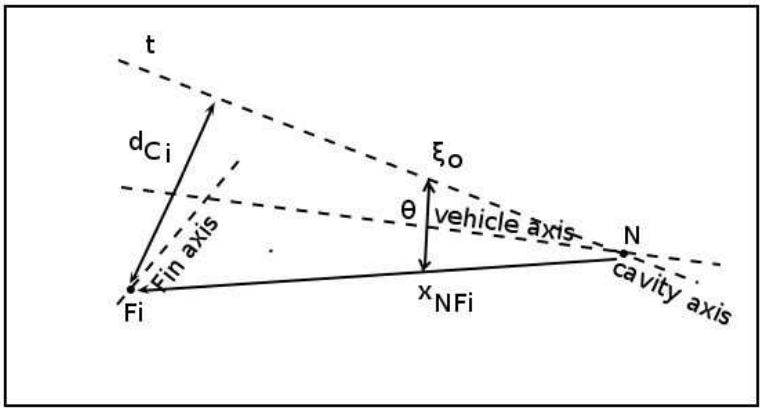

Figure 9. Calculation of fin penetration depth.

3.3 Tail cavity interactions

We now consider tail slap interactions and assume that these short impacts are elastic. It is seen that interaction force is proportional to penetration distance D_t (for tail) :

$$S_I = K(D_t)D_t$$

and it is directed along perpendicular to cavity axis at the impact point, which is pointed inward towards the cavity.

$$K(D_t) = K_0 \; if \; D_t \geq 0,$$

and

$$K(D_t) = 0 \; if \; D_t \leq 0$$

Here K_0 is known as 'equivalent stiffness' and has been determined experimentally.

3.4 Fin forces calculations

The fins are controlled to provide lift in the after-body section and to maneuver the vehicle. We consider a 4-fin configuration as shown in Figure 4. Each fin interacts with the surrounding fluid with forces that depend on the immersion depth in the fluid, the velocity at the fin location with respect to the fluid, the fin geometry and the angle of attack. Here the forces are first expressed in a reference frame $F_{Fi,fi}$, with origin F_i and triad $f_i = (f_1, f_2, f_3)$ fixed to ith fin as shown in Fig. 10.

Triad $f_i$is obtained by a rotation that brings β into the undeflected fin configuration $f_i = (f_1, f_2, f_3)$, $f_k = R_i b_k$, $k = 1, 2, 3$. The total rotation from β to f_i is hence

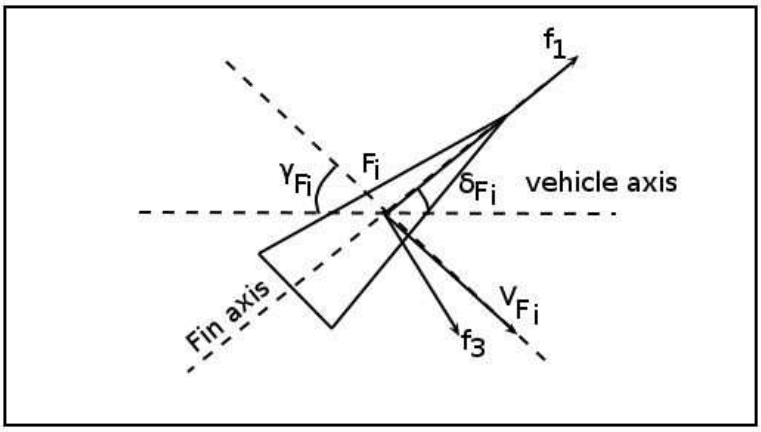

Figure 10. Details of fin and frames attached to fins.

$$f_k = R_{\beta \to f_i} b_k$$

and

$$R_{\beta \to f_i} = R(\delta_{F_i}, f_2) R_i$$

In the fin fixed reference system, the forces are determined in terms of the angle of attack and the

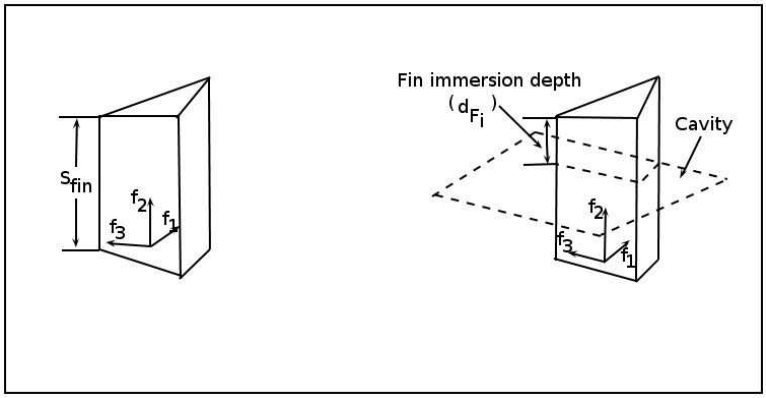

Figure 11. Fin fixed frame and fin velocity.

immersion depth. For a wedge shaped fin, the force components on the ith fin is given by,

$$S_{Fi}^{fi} = \frac{1}{2} \rho V_{Fi}^2 S \left\{ C_x(\gamma_{Fi}, d_{Fi}); C_y(\gamma, d_{Fi}); C_z(\gamma_{Fi}, d_{Fi}) \right\}^T ,$$

Here V_{Fi} is the magnitude of the velocity vector in the fin frame origin fi. S is the fin surface area and C_x, C_y, C_z are force coefficients defined in terms of angle of attack and penetration distance.

The behaviour of force coeficients with varying angle of attacks are evident from following plots.

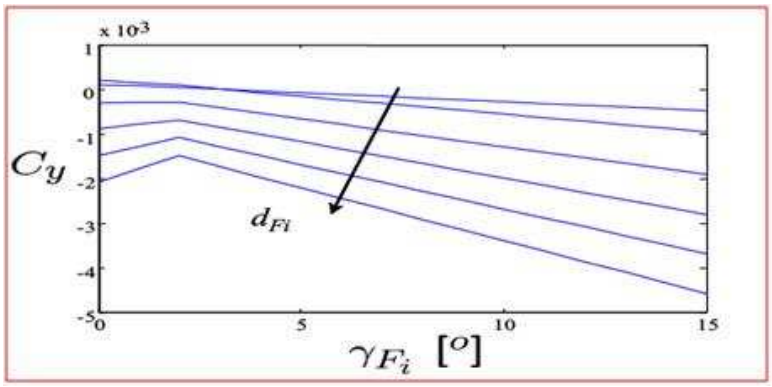

Figure 12. Fin force coefficients vs angle of attack, for different penetration depths.

4. RESULTS

Analyzing the above graphs, a bilinear behavior of the force coefficients for given penetration depth is seen. They show that the force coefficients are associated with two flow regimes. The first flow regime occurs at low angle of attack when two separate cavities are formed at the base and at the leading edge. For larger angle of attack the two cavities merge to form a supercavity that envelopes all the surface. However, the tail cavity interactions that we have done here needs more rigorous mathematical treatment. No planing has been considered in this case. Planing is a large force exerted when suddenly vehicle body interacts with cavity.

5. CONCLUSIONS

The present study is an initial effort towards understanding supercavitation and dynamics of a supercavitating vehicle. Supercavitating vehicles are characterized by substantially reduced hydrodynamic drag, in comparison with fully wetted underwater vehicles. Drag is localized at the nose of the vehicle, where a cavitator generates a cavity that completely envelopes the body, at the fins, and on the vehicle after-body. The body is acted upon by a system of forces corresponding to the interaction of the vehicle control surfaces with the cavity boundaries. The control surfaces include the fins at the back of the vehicle and the cavitator, whose primary function is the generation of the supercavity. The control surfaces support the vehicle in the vertical direction by providing lift, and allow for roll, pitch and yaw control. We have used a simple approach to calculate the underlying forces in a supercavitating vehicle. We did the calculations, assuming there is no planing force which needs more rigorous mathematical treatment and this forms a scope for future research on the dynamics of supercavitating vehicle.

Acknowledgements

This project is done is under the guidance of Prof. A.K. Ghosh, Department of Aerospace Engineering, IIT Kanpur. I am very grateful to him for his kind guidance and support throughout the project. I also acknowledge Prof. Prasanta K. Panigrahi for his valuable suggestions for the improvement of the project. I also thank S.K. Burnwal, M.tech student IIT-K for his encouragement and guidance during the project.

References

[1] Trajectory Optimization Strategies for Supercavitating Underwater Vehicles, M. Ruzzene, R. Kamada, C.L. Bottasso and F. Scorcelletti, Journal of Vibration and Control 2008; 14; 611

[2] A benchmark control problem for supercavitating vehicles and an initial investigation of solutions, J. Dzielski and A. Kurdila, Journal of Vibration and Control 9, 791-804 (2003).

[3] Fundamentals of cavitation - Franc and Michel, Kluwer Academic Publishers, New York.

[4] Racing Through Water: Supercavitation V. Sturgeon, Caltech Undergraduate Research Journal, Vol. 1, No. 2, 16-21 (2001).

P R A Y A S
Students' Journal
of Physics

PROBLEMS IN PHYSICS

Readers are invited to submit the solutions of the problems in this section within two months. Correct solutions, along with the names of the senders, will be published in the alternate issues. Solutions should be sent to: H.S. Mani, c/o A.M. Srivastava, Institute of Physics, Bhubaneswar, 751005; e-mail: ajit@iopb.res.in

Communicated by H.S. Mani

1. The vector potential is defined by the equation $\vec{B} = \vec{\bigtriangledown} \times \vec{A}$ and by applying Stokes theorem we see that the loop integral $\int_c \vec{A}.\vec{dl}$ = $\int \vec{B}.\vec{dS}$ where the surface integral is over an area with its boundary as the loop c (with the contour c being in the counter clock-wise direction.This is the magnetic flux enclosed by the closed loop c. This is true irrespective of the size of the loop.

   Consider now the case of a thin current carrying solenoid situated on earth, with flux ϕ through it. The loop c surrounding the solenoid is taken to be circular, concentric with solenoid, and has radius R. Take R to be extremely large, say distance to the moon. The above expression tells us that as soon as the flux ϕ is changed on the earth, $\vec{A}$ on the loop (at distance R away from the solenoid) must change instantaneously. How is this consistent with Special Relativity?

   This problem was raised in a Physics Open Discussion session at IOP Bubaneswar, by Mr. K.V. Shuddhodan and few other students from class XII DAV school.

Problems set by H.S. Mani

2. Consider two one-dimensional coupled simple harmonic oscillators described by the Hamiltonian

$$H = \frac{p_1^2}{2m_1} + \frac{p_2^2}{2m_2} + \frac{1}{2}(k_1\, x_1^2 + k_2^2\, x_2^2 + k_{12}\, x_1\, x_2)$$

   Find the energy levels of the system.(here p_1, p_2, x_1, x_2) refer to the momenta and coordinates of the two harmonic oscillators respectively. m_1, m_2 are their respective masses.)

Solutions to the problems given in Vol.4 No.2

Problem 1: Suppose you are standing at the centre of a circular palm groove with uniform density of 4 trees per 100 square meter and the breadth of each tree is half a meter. Find
(a) the radius R of the groove for which your horizon is completely covered by trees,
(b) The radius $R_{1/2}$of the groove for which half of your horizon is covered by the trees,
(c) the general formula connecting the radius of the groove R to the fraction of your horizon covered by trees.

Note: this is the two-dimensional analogue of the famous Olber's paradox, dating back to 1826 - i.e., why is the sky dark at night? the answer came over a hundred years later from the Big Bang cosmology, showing that the visible universe has a finite radius of about 14 billion light years.

Solution to Problem 1: *Solution for the first part is given by Mr. Himanshu Raj, 3rd year Physics, NISER, Bhubaneswar. Full solution is given by D.P. Roy*

If a tree is at a distance of r from the observer the angle subtended by the tree is b/r radians. The number of trees between a distance r and $r+dr$ is $2\,\pi\,r\,dr\,\rho$ where ρ is the density of trees (number of trees per unit area). Hence the angle subtended by the trees between r and $r+dr$ is $2\,\pi\,b\,\rho\,dr$, assuming no overlap then the distance R for which complete cover occurs is given by

$$2\,\pi\,\rho\,b\int_0^R dr = 2\,\pi$$

$$R = \frac{1}{\rho\,b} = 50m$$

To include overlapof trees we proceed iteratively. As a first iteration, the number of trees within a radius r already subtend an angle $2\,\pi\,b\,\rho\,r$ and we write

$$2\,\pi\,b\,\rho\int_0^R dr\,(1-\rho\,br) = 2\pi$$

leading to

$$\rho\,b\,R - \frac{(\rho\,b\,R)^2}{2} = 1$$

This iteration can be repeated infinite times leading to

$$[\rho\,b\,R - \frac{(\rho\,b\,R)^2}{2} + \frac{(\rho\,b\,R)^3}{3!} - \ldots] = [1 - e^{-\rho\,b\,R}] = 1$$

Thus (a) full coverage happens only for $R=\infty$ and(b) half coverage happens when $R_{1/2} = \frac{\ln(2)}{\rho\,b} \approx 30m$.

(c)The general formula for a fraction f covered is

$$R_f = \frac{1}{\rho\,b} ln(\frac{1}{1-f})$$